11

Minimum-Energy Motion Planning for Differential-Driven Wheeled Mobile Robots

Chong Hui Kim[1] and Byung Kook Kim[2]
[1]*Agency for Defense Development,*
[2]*School of Electrical Engineering and Computer Science, KAIST*
Republic of Korea

1. Introduction

With the remarkable progresses in robotics, mobile robots can be used in many applications including exploration in unknown areas, search and rescue, reconnaissance, security, military, rehabilitation, cleaning, and personal service. Mobile robots should carry their own energy source such as batteries which have limited energy capacity. Hence their applications are limited by the finite amount of energy in the batteries they carry, since a new supply of energy while working is impossible, or at least too expensive to be realistic. ASIMO, Honda's humanoid robot, can walk for only approximately 30 min with its rechargeable battery backpack, which requires four hours to recharge (Aylett, 2002). The BEAR robot, designed to find, pick up, and rescue people in harm's way, can operate for approximately 30 min (Klein et al., 2006). However, its operation time is insufficient for complicated missions requiring longer operation time. Since operation times of mobile robots are mainly restricted by the limited energy capacity of the batteries, energy conservation has been a very important concern for mobile robots (Makimoto & Sakai, 2003; Mei et al., 2004; Spangelo & Egeland, 1992; Trzynadlowski, 1988; Zhang et al., 2003). Rybski et al. (Rybski et al., 2000) showed that power consumption is one of the major issues in their robot design in order to survive for a useful period of time.

Mobile robots usually consist of batteries, motors, motor drivers, and controllers. Energy conservation can be achieved in several ways, for example, using energy-efficient motors, improving the power efficiency of motor drivers, and finding better trajectories (Barili et al., 1995; Mei et al., 2004; Trzynadlowski, 1988; Weigui et al., 1995). Despite efficiency improvements in the motors and motor drivers (Kim et al., 2000; Leonhard, 1996), the operation time of mobile robots is still limited in their reliance on batteries which have finite energy. We performed experiments with mobile robot called Pioneer 3-DX (P3-DX) to measure the power consumption of components: two DC motors and one microcontroller which are major energy consumers. Result shows that the power consumption by the DC motors accounts for more than 70% of the total power. Since the motor speed is largely sensitive to torque variations, the energy dissipated by a DC motor in a mobile robot is critically dependent on its velocity profile. Hence energy-optimal motion planning can be achieved by determining the optimal velocity profile and by controlling the mobile robot to follow that trajectory, which results in the longest working time possible.

The total energy drawn from the batteries is converted to mechanical energy by driving motors, which is to induce mobile robot's motion with some losses such as armature heat dissipation by the armatures in the motors. The DC motor is most widely used to produce mechanical power from electric power. It converts electric power into mechanical power during acceleration and cruise. Moreover, during deceleration, mechanical energy can be converted back to electrical energy (Electro-Craft, 1977). However, the motor is not an ideal energy converter, due to losses caused by the armature resistance, the viscous friction, and many other loss components. Many researchers have concentrated on minimizing losses of a DC motor (Trzynadlowski, 1988; Angelo et al., 1999; Egami et al., 1990; El-satter et al., 1995; Kusko & Galler, 1983; Margaris et al., 1991; Sergaki et al., 2002; Tal, 1973). They developed cost function in terms of the energy loss components in a DC motor in order to conserve limited energy. The loss components in a DC motor include the armature resistance loss, field resistance loss, armature iron loss, friction and windage losses, stray losses, and brush contact loss. Since it is difficult to measure all the parameters of the loss components, its implementation is relatively complex. To overcome this problem, some researches considered only the armature resistance loss as a cost to be minimized (Trzynadlowski, 1988; Tal, 1973; Kwok & Lee, 1990). However, loss-minimization control is not the optimal in terms of the total energy drawn from the batteries.

Control of wheeled mobile robot (WMR) is generally divided into three categories (Divelbiss & Wen, 1997).

- *Path Planning*: To generate a path off-line connecting the desired initial and final configurations with or without obstacle avoidance.
- *Trajectory Generation*: To impose a velocity profile to convert the path to a trajectory.
- *Trajectory Tracking*: To make a stable control for mobile robots to follow the given trajectory.

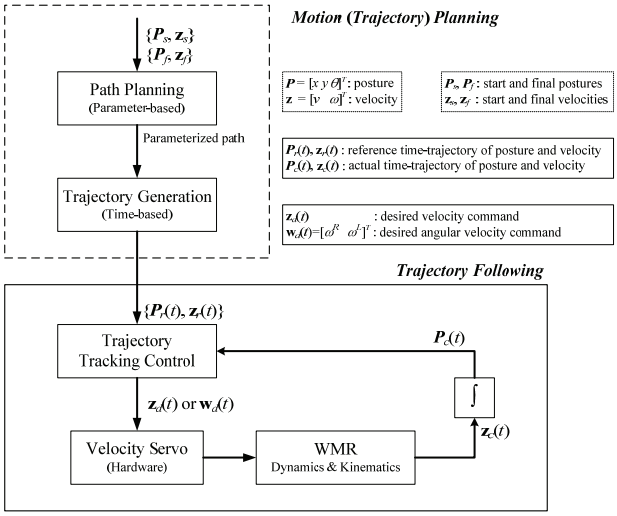

Figure 1. Traditional overall scheme of WMR control

Trajectory means a time-based profile of position and velocity from start to destination while paths are based on non-time parameters. Fig. 1 shows the overall control architecture

of WMR system (Choi, 2001). Finding a feasible trajectory is called trajectory planning or motion planning (Choset et al., 2005).

Trajectory planning (motion planning) is a difficult problem since it requires simultaneously solving the path planning and velocity planning (trajectory generation) problems (Fiorini & Shiller, 1998). Most of the paths of WMR consist of straight lines and arcs. The pioneering work by Dubins (Dubins, 1957) and then by Reeds and Shepp (Reeds & Shepp, 1990) showed that the shortest paths for car-like vehicle were made up of straight lines and circular arcs. Since these paths generate discontinuities of curvature at junctions between line and arc segment, a real robot would have to stop at each curvature discontinuity. Hence frequent stops and turnings cause unnecessary acceleration and deceleration that consume significant battery energy. In order to remove discontinuity at the line-arc transition points, several types of arcs have been proposed. Clothoid and cubic spirals provide smooth transitions (Kanayama & Miyake, 1985; Kanayama & Harman, 1989). However, these curves are described as functions of the path-length and it is hard to consider energy conservation and dynamics of WMR. Barili et al. described a method to control the travelling speed of mobile robot to save energy (Barili et al., 1995). They considered only straight lines and assumed constant acceleration rate. Mei et al. presented an experimental power model of mobile robots as a function of constant speed and discussed the energy efficiency of the three specific paths (Mei et al., 2004; Mei et al., 2006). They did not consider arcs and the energy consumption in the transient sections for acceleration and deceleration to reach a desired constant speed.

In this book chapter, we derive a minimum-energy trajectory for differential-driven WMR that minimizes the total energy drawn from the batteries, using the actual energy consumption from the batteries as a cost function. Since WMR mainly moves in a straight line and there is little, if any, rotation (Barili et al., 1995; Mei et al., 2005), first we investigate *minimum-energy translational trajectory generation problem* moving along a straight line. Next we also investigate *minimum-energy turning trajectory planning problem* moving along a curve since it needs turning trajectory as well as translational trajectory to do useful actions. To demonstrate energy efficiency of our trajectory planner, various simulations are performed and compared with loss-minimization control minimizing armature resistance loss. Actual experiments are also performed using a P3-DX mobile robot to validate practicality of our algorithm.

The remainder of the book chapter is organized as follows. Section 2 gives the kinematic and dynamic model of WMR and energy consumption model of WMR. In Section 3, we formulate the minimum-energy translational trajectory generation problem. Optimal control theory is used to find the optimal velocity profile in analytic form. Experimental environment setup to validate simulation results is also presented. In Section 4, we formulate the minimum-energy turning trajectory planning problem and suggest iterative search algorithm to find the optimal trajectory based on the observation of the cost function using the solution of Section 3. Finally, we conclude with remarks in Section 5.

2. WMR Model

2.1 Kinematic and Dynamic Model of WMR

It is well known that a WMR is a nonholonomic system. A full dynamical description of such nonholonomic mechanical system including the constraints and the internal dynamics can be found in (Campion et al., 1991). Yun (Yun, 1995; Yun & Sarkar, 1998) formulated a dynamic system with both holonomic and nonholonomic constraints resulting from rolling contacts into the standard control system form in state space. Kinematic and dynamic

modeling of WMRs has been addressed by several researches. A systermatic procedure for kinematic model derivation can be found in (Alexander & Maddocks, 1989; Muir & Neuman, 1987). Campion et al. (Campion et al., 1996) have given a general and unifying presentation of the modeling issue of WMR with an arbitrary number of wheeles of various types and various motorizations. They have pointed out the structural properties of the kinematic and dynamic models taking into account the restriction to the robot mobility induced by constraints.

Unlike car-like robot (Jiang et al., 1996; Laumond et al., 1994; Laumond et al., 1998), we assumed that a WMR has a symmetric structure driven by two identical DC motors, as shown in Fig. 2. Define the posture (position x, y and orientation θ) as $\boldsymbol{P}(t)=\left[x(t) \quad y(t) \quad \theta(t)\right]^T$, the translational velocity of a WMR as v, and its rotational velocity as ω. Then the WMR's kinematics is defined by

$$\begin{bmatrix} \dot{x} \\ \dot{y} \\ \dot{\theta} \end{bmatrix} = \mathbf{T}_P \begin{bmatrix} v \\ \omega \end{bmatrix}, \mathbf{T}_P = \begin{bmatrix} \cos\theta & 0 \\ \sin\theta & 0 \\ 0 & 1 \end{bmatrix} \tag{1}$$

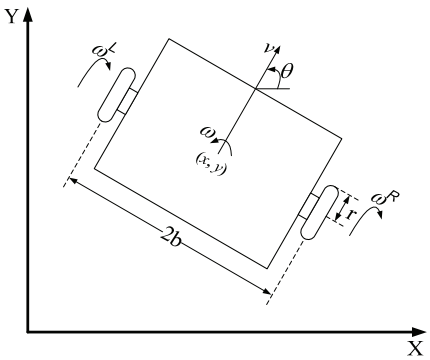

Figure 2. Structure of WMR

Assume that two identical DC motors have the same armature resistance R_a, back-emf constant K_b, and gear ratio n. To simplify dynamics, we ignore the inductance of the armature circuits because the electrical response is generally much faster than the mechanical response. Letting V_s be the battery voltage, the armature circuits of both motors are described as

$$R_a\mathbf{i} = V_s\mathbf{u} - K_b n\mathbf{w} \tag{2}$$

where $\mathbf{i}=\left[i^R \quad i^L\right]^T$ is the armature current vector, $\mathbf{w}=\left[\omega^R \quad \omega^L\right]^T$ is the angular velocity vector of the wheeles, and $\mathbf{u}=\left[u^R \quad u^L\right]^T$ is the normalized control input vector. Superscripts R and L correspond to right and left motors, respectively.

In addition, the dynamic relationship between angular velocity and motor current, considering inertia and viscous friction, becomes (Yun & Yamamoto, 1993)

$$\mathbf{J}\frac{d\mathbf{w}}{dt} + F_v\mathbf{w} = K_t n\mathbf{i} \tag{3}$$

where F_v is the viscous friction coefficient and equivalent inertia matrix of motors $\mathbf{J}$ is $\mathbf{J} = \mathbf{S}^T\mathbf{M}\mathbf{S}$, which is 2x2 symmetric.
From Eqs. (2) and (3), we obtain the following differential equation.

$$\dot{\mathbf{w}} + \mathbf{A}\mathbf{w} = \mathbf{B}\mathbf{u} \tag{4}$$

where

$$\mathbf{A} = \begin{bmatrix} a_1 & a_2 \\ a_2 & a_1 \end{bmatrix} = \mathbf{J}^{-1}\left(F_v + \frac{K_t K_b n^2}{R_a}\right),\ \mathbf{B} = \begin{bmatrix} b_1 & b_2 \\ b_2 & b_1 \end{bmatrix} = \mathbf{J}^{-1}\frac{V_s K_t n}{R_a}$$

Define a state vector as $\mathbf{z} = \begin{bmatrix} v & \omega \end{bmatrix}^T$. Then v and ω are related to ω^R and ω^L by

$$\mathbf{z} = \begin{bmatrix} v \\ \omega \end{bmatrix} = \mathbf{T}_q \begin{bmatrix} \omega^R \\ \omega^L \end{bmatrix} = \mathbf{T}_q\mathbf{w},\ \mathbf{T}_q = \begin{bmatrix} r/2 & r/2 \\ r/2b & -r/2b \end{bmatrix} \tag{5}$$

Using the similarity transformation, from Eqs. (4) and (5), we obtain the following equation

$$\dot{\mathbf{z}} + \bar{\mathbf{A}}\mathbf{z} = \bar{\mathbf{B}}\mathbf{u} \tag{6}$$

where

$$\bar{\mathbf{A}} = \mathbf{T}_q\mathbf{A}\mathbf{T}_q^{-1} = \begin{bmatrix} \pi_v & 0 \\ 0 & \pi_\omega \end{bmatrix} = \begin{bmatrix} a_1 + a_2 & 0 \\ 0 & a_1 - a_2 \end{bmatrix}$$

$$\bar{\mathbf{B}} = \mathbf{T}_q\mathbf{B} = \begin{bmatrix} \beta_1 & \beta_1 \\ \beta_2 & -\beta_2 \end{bmatrix} = \begin{bmatrix} r(b_1 + b_2)/2 & r(b_1 + b_2)/2 \\ r(b_1 - b_2)/2b & -r(b_1 - b_2)/2b \end{bmatrix}$$

The overall dynamics of a WMR is shown in Fig. 3, where I_2 is the 2x2 unit matrix.

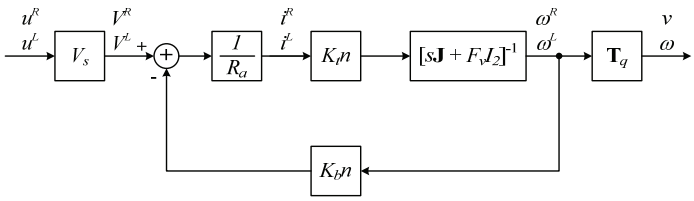

Figure 3. Block diagram of WMR

2.2 Energy Consumption of WMR

The energy drawn from the batteries is converted to mechanical energy to drive motors and losses such as the heat dissipation in the armature resistance. In a WMR, energy is

dissipated by the internal resistance of batteries, amplifier resistance in motor drivers, armature resistance, and viscous friction of motors. Fig. 4 shows a simplified circuit diagram of a WMR system.

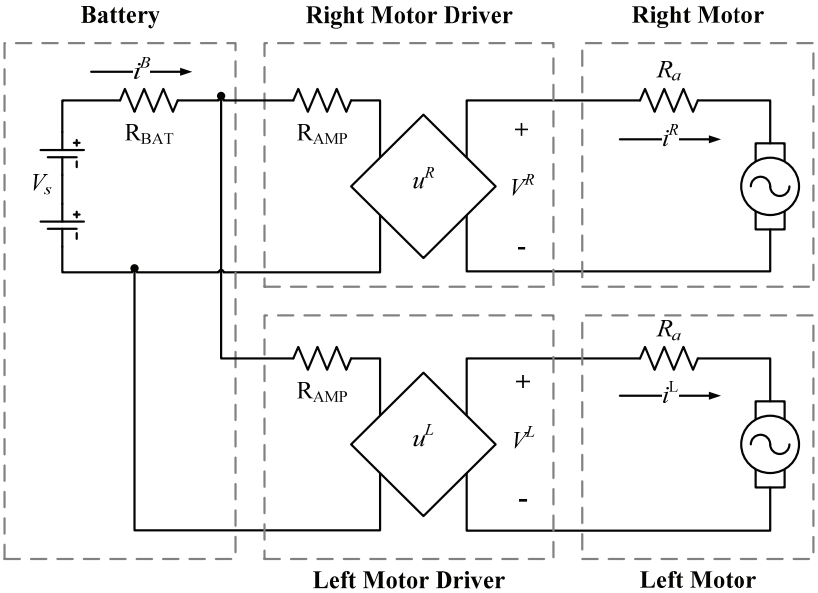

Figure 4. Circuit diagram of batteries, motor drivers, and motors of WMR

A pulse width modulated (PWM) controller is the preferred motor speed controller because little heat is generated and it is energy efficient compared to linear regulation (voltage control) of the motor. We assume that an H-bridge PWM amplifier is used as a motor driver, and this is modeled by its amplifier resistance R_{AMP} and PWM duty ratio u^R and u^L. In our robot system, P3-DX, internal resistance of battery (CF-12V7.2) is approximately 22mΩ and power consumption by the motor drivers is 0.2W. Since internal resistance of battery is much smaller compared with armature resistance of motor (710mΩ) and the power consumption by the motor drivers is much smaller than that of motors (several watts), they are ignored here. Hence the total energy supplied from the batteries to the WMR, E_W, is the cost function to be minimized and is defined as

$$E_W = \int \mathbf{i}^T \mathbf{V} dt = V_s \int \mathbf{i}^T \mathbf{u} dt \tag{7}$$

where $\mathbf{V} = \begin{bmatrix} V^R & V^L \end{bmatrix}^T$ is the input voltage applied to the motors from the batteries, and $\mathbf{u} = \mathbf{V} / V_s = \begin{bmatrix} u^R & u^L \end{bmatrix}^T$.

As there is a certain limit on a battery's output voltage, WMR systems have a voltage constraint on batteries:

$$-u^{\max} \le u^R \le u^{\max}, \; -u^{\max} \le u^L \le u^{\max} \tag{8}$$

From Eqs. (2) and (5), E_W can be written in terms of the velocity and the control input as

$$E_W = \int \left(k_1 \mathbf{u}^T \mathbf{u} - k_2 \mathbf{z}^T \mathbf{T}_q^{-T} \mathbf{u} \right) dt \tag{9}$$

where $k_1 = V_s^2 / R_a$ and $k_2 = K_b n V_s / R_a$.
From Eqs. (2) and (3), the cost fuction E_W becomes

$$E_W = R_a \int \mathbf{i}^T \mathbf{i} dt + F_v \frac{K_b}{K_t} \int \mathbf{z}^T \mathbf{T}_q^{-T} \mathbf{T}_q^{-1} \mathbf{z} dt + \frac{K_b}{K_t} \int \dot{\mathbf{z}}^T \mathbf{T}_q^{-T} \mathbf{J}^T \mathbf{T}_q^{-1} \mathbf{z} dt \tag{10}$$

Note that the first term, $E_R \left(= R_a \int \mathbf{i}^T \mathbf{i} dt \right)$, is the energy dissipated by the armature resistance in the motors and the cost function of loss-minimization control considering only the armature resistance loss. The second term, $E_F \left(= F_v \frac{K_b}{K_t} \int \mathbf{z}^T \mathbf{T}_q^{-T} \mathbf{T}_q^{-1} \mathbf{z} dt \right)$, corresponds to the velocity sensitive loss due to viscous friction. The last term, $E_K \left(= \frac{K_b}{K_t} \int \dot{\mathbf{z}}^T \mathbf{T}_q^{-T} \mathbf{J}^T \mathbf{T}_q^{-1} \mathbf{z} dt \right)$, is the kinetic energy stored in the WMR and will have zero average value when the velocity is constant or final velocity equal to the initial velocity. This means that the net contribution of the last term to the energy consumption is zero.

3. Minimum-Energy Translational Trajectory Generation

A mobile robot's path usually consists of straight lines and arcs. In the usual case, a mobile robot mainly moves in a straight line and there is little, if any, rotation (Barili et al., 1995; Mei et al., 2005). Since the energy consumption associated with rotational velocity changes is much smaller than the energy consumption associated with translational velocity changes, we investigate minimum-energy translational trajectory generation of a WMR moving along a straight line. Since the path of WMR is determined as a straight line, this problem is reduced to find velocity profile minimizing energy drawn from the batteries.

3.1 Problem Statement

The objective of optimal control is to determine the control variables minimizing the cost function for given constraints. Because the rotational velocity of WMR, ω, is zero under translational motion constraint, let $\boldsymbol{P}(t) = \begin{bmatrix} x(t) & 0 & 0 \end{bmatrix}^T$ be the posture and $\mathbf{z}(t) = \begin{bmatrix} v(t) & 0 \end{bmatrix}^T$ be the velocity at time t. Then the *minimum-energy translational trajectory generation problem* investigated in this section can be formulated as follows.
Problem: Given initial and final times t_0 and t_f, find the translational velocity $v(t)$ and the control input $u(t)$ which minimizes the cost function

$$E_W = \int_{t_0}^{t_f} \left(k_1 \mathbf{u}^T \mathbf{u} - k_2 \mathbf{z}^T \mathbf{T}_q^{-T} \mathbf{u} \right) dt$$

for the system described by Eq. (6) subject to

(1) initial and final postures: $\boldsymbol{P}(t_0)=\begin{bmatrix}x_0 & 0 & 0\end{bmatrix}^T$ and $\boldsymbol{P}(t_f)=\begin{bmatrix}x_f & 0 & 0\end{bmatrix}^T$,

(2) initial and final velocities: $\mathbf{z}(t_0)=\begin{bmatrix}v_s & 0\end{bmatrix}^T$ and $\mathbf{z}(t_f)=\begin{bmatrix}v_f & 0\end{bmatrix}^T$, and

(3) satisfying the batteries' voltage constraints, $u^{\max}$

As time is not critical, a fixed final time is used.

3.2 Minimum-Energy Translational Trajectory

Without loss of generality, we assume that the initial and final velocities are zero, and the initial posutre is zero. Then the *minimum-energy translational trajectory generation problem* can be written as

$$\text{minimize } E_W=\int_0^{t_f}\left(k_1\mathbf{u}^T\mathbf{u}-k_2\mathbf{z}\mathbf{T}_q^{-T}\mathbf{u}\right)dt \tag{11}$$

$$\text{subject to} \qquad \dot{\mathbf{z}}=-\bar{\mathbf{A}}\mathbf{z}+\bar{\mathbf{B}}\mathbf{u} \tag{12}$$

$$\mathbf{z}(0)=\mathbf{z}(t_f)=\begin{bmatrix}0 & 0\end{bmatrix}^T \tag{13}$$

$$P_f=\int_0^{t_f}\mathbf{T}_P\mathbf{z}dt=\begin{bmatrix}x_f & 0 & 0\end{bmatrix}^T \tag{14}$$

$$\begin{bmatrix}-u^{\max}\\-u^{\max}\end{bmatrix}\le\mathbf{u}=\begin{bmatrix}u^R\\u^L\end{bmatrix}\le\begin{bmatrix}u^{\max}\\u^{\max}\end{bmatrix} \tag{15}$$

We used the Pontryagin's Maximum Principle to find the minimum-energy velocity profile that minimizes Eq. (11) while satisfying the constraints in Eqs. (13) – (15) for the system, with Eq. (12). Let the Largrange multiplier for the posture constraint, Eq. (14), be $\boldsymbol{\alpha}=\begin{bmatrix}a_x & a_y & a_\theta\end{bmatrix}^T$. Defining the multipler function for Eq. (12) as, $\boldsymbol{\lambda}=\begin{bmatrix}\lambda_v & \lambda_\omega\end{bmatrix}^T$, the Hamiltonian H is

$$H=k_1\mathbf{u}^T\mathbf{u}-k_2\mathbf{z}^T\mathbf{T}_q^{-T}\mathbf{u}-\boldsymbol{\alpha}^T\mathbf{T}_p\mathbf{z}+\boldsymbol{\alpha}^T\boldsymbol{P}_f/t_f+\boldsymbol{\lambda}^T\left(-\bar{\mathbf{A}}\mathbf{z}+\bar{\mathbf{B}}\mathbf{u}\right) \tag{16}$$

The necessary conditions for the optimal velocity $\mathbf{z}^*$ and the control input $\mathbf{u}^*$ are

$$\partial H/\partial\mathbf{u}=2k_1\mathbf{u}-k_2\mathbf{T}_q^{-1}\mathbf{z}+\bar{\mathbf{B}}^T\boldsymbol{\lambda}=0 \tag{17}$$

$$\partial H/\partial\mathbf{z}=-k_2\mathbf{T}_q^{-T}\mathbf{u}-\mathbf{T}_P^T\boldsymbol{\alpha}-\bar{\mathbf{A}}^T\boldsymbol{\lambda}=-\dot{\boldsymbol{\lambda}} \tag{18}$$

$$\partial H/\partial\boldsymbol{\lambda}=-\bar{\mathbf{A}}\mathbf{z}+\bar{\mathbf{B}}\mathbf{u}=\dot{\mathbf{z}} \tag{19}$$

From Eqs. (17) – (19), we obtain the following differential equation.

$$\ddot{\mathbf{z}}-\left(\bar{\mathbf{B}}\bar{\mathbf{B}}^T\bar{\mathbf{A}}^T\bar{\mathbf{B}}^{-T}\bar{\mathbf{B}}^{-1}\bar{\mathbf{A}}-\frac{k_2}{k_1}\bar{\mathbf{B}}\bar{\mathbf{B}}^T\mathbf{T}_q^{-T}\bar{\mathbf{B}}^{-1}\bar{\mathbf{A}}\right)\mathbf{z}+\frac{1}{2k_1}\bar{\mathbf{B}}\bar{\mathbf{B}}^T\mathbf{T}_P^T\boldsymbol{\alpha}=0 \tag{20}$$

As $\bar{\mathbf{B}}\bar{\mathbf{B}}^T$ and $\bar{\mathbf{A}}$ are diagonal matrices, Eq. (20) is reduced to quadratic differential form as follows.

$$\ddot{\mathbf{z}} - \mathbf{Q}^T\mathbf{Q}\mathbf{z} + \mathbf{R}^T\mathbf{T}_P^T\boldsymbol{\alpha} = 0 \tag{21}$$

where $\mathbf{Q}^T\mathbf{Q} = \bar{\mathbf{A}}^T\bar{\mathbf{A}} - \frac{k_2}{k_1}\bar{\mathbf{B}}\bar{\mathbf{B}}^T\mathbf{T}_q^{-T}\bar{\mathbf{B}}^{-1}\bar{\mathbf{A}}$, $\mathbf{Q} = \begin{bmatrix} 1/\tau_v & 0 \\ 0 & 1/\tau_\omega \end{bmatrix}$, and $\mathbf{R} = \frac{\bar{\mathbf{B}}^T\bar{\mathbf{B}}}{2k_1} = \begin{bmatrix} \eta_v & 0 \\ 0 & \eta_\omega \end{bmatrix}$. Here $\tau_v = (J_1 + J_2)/\sqrt{F_v(F_v + K_tK_bn^2/R_a)}$ denotes the mechanical time constant for translation and $\tau_\omega = (J_1 - J_2)/\sqrt{F_v(F_v + K_tK_bn^2/R_a)}$ denotes the mechanical time constant for rotation of WMR. Since we ignore energy dissipation associated with rotational velocity changes and consider only a WMR moving along a straight line (i.e., rotational velocity is zero), the optimal velocity $\mathbf{z}^*$ becomes

$$\mathbf{z}^*(t) = \begin{bmatrix} v^*(t) \\ \omega^*(t) \end{bmatrix} = \begin{bmatrix} C_1e^{t/\tau_v} + C_2e^{-t/\tau_v} + K_v \\ 0 \end{bmatrix} \tag{22}$$

where

$$C_1 = \frac{e^{-t_f/\tau_v} - 1}{e^{t_f/\tau_v} - e^{-t_f/\tau_v}}K_v,\ C_2 = \frac{1 - e^{t_f/\tau_v}}{e^{t_f/\tau_v} - e^{-t_f/\tau_v}}K_v,\ K_v = \frac{x_f\left(e^{t_f/\tau_v} - e^{-t_f/\tau_v}\right)}{2\tau_v\left(2 - e^{t_f/\tau_v} - e^{-t_f/\tau_v}\right) + t_f\left(e^{t_f/\tau_v} - e^{-t_f/\tau_v}\right)}$$

To investigate the properties of the minimum-energy velocity profile, the minimum-energy translational velocity profile, Eq. (22), is shown in Fig. 5 as velocity per unit versus time per unit, where the reference velocity is taken as the x_f/t_f ratio and the reference time t/t_f for various $k = \tau_v/t_f$ (the ratio of translational mechanical time constant per displacement time) using the parameters shown in Table 1.

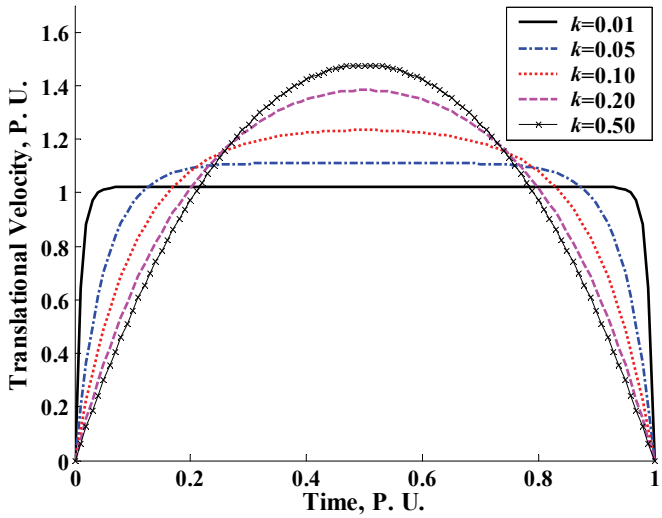

Figure 5. Minimum-Energy velocity profiles for incremental motion at various $k = \tau_v/t_f$

Parameter	Value	Parameter	Value
R_a	0.71Ω	K_t	0.023Nm/A
K_b	0.023V/(rad/s)	n	38.3
m_c	13.64Kg	m_ω	1.48Kg
V_s	12.0V	$u^{\max}$	1.0
F_v	0.039Nm/(rad/s)	r	0.095m
b	0.165m	$\mathbf{J}=\begin{bmatrix} J_1 & J_2 \\ J_2 & J_1 \end{bmatrix}$	$\begin{bmatrix} 0.0799 & 0.0017 \\ 0.0017 & 0.0799 \end{bmatrix}$

Table 1. Parameters of the WMR, P3-DX

This shows that for k close to zero the minimum-energy velocity profile resembles a widely used trapezoidal velocity profile, whereas for values of $k > 0.2$ the profile rapidly converges to a parabolic profile instead of the widely used trapezoidal profile. As shown in Fig. 5, the minimum-energy velocity profile has a symmetric form for the *minimum-energy translational trajectory generation problem*, of Eqs. (11) – (15) as follows.

$$v^*(t) = \frac{x_f}{\tau_v} \frac{\sinh\left(t_f/\tau_v\right) - \sinh\left(\left(t_f - t\right)/\tau_v\right) - \sinh\left(t/\tau_v\right)}{2\left(1-\cosh\left(t_f/\tau_v\right)\right) + \frac{t_f}{\tau_v}\sinh\left(t_f/\tau_v\right)} \tag{23}$$

Eq. (23) means that the minimum-energy velocity profile depends on the ratio of the mechanical time constant τ_v and the displacement time t_f.

3.3 Simulations and Experiments

3.3.1 Simulations

Several simulations were performed to evaluate the energy saving of the minimum-energy control optimizing the cost function E_W of Eq. (11); these were compared with two results of other methods: loss-minmization control (Trzynadlowski, 1988; Tal, 1973; Kwok & Lee, 1990) optimizing energy loss due to armature resistance of a DC motor, $E_R\left(= R_a \int \mathbf{i}^T \mathbf{i} dt\right)$, and the fixed velocity profile of commonly used trapezoidal velocity profile optimizing the cost function E_W of Eq. (11).

Table 3.2 shows the simulation results of the energy saving for various displacements x_f and displacement time t_f. *Minimum-Energy* denotes the mnimum-energy control optimizing the cost fucntion E_W, *Loss-Minimization* denotes the loss-minimization control optimizing the cost function E_R, and *TRAPE* denotes the trapezoidal velocity profile optimizing the cost fuction E_W. Values in parenthesis represent percentage difference in the total energy drawn from the batteries with respect to that of minimum-energy control. It shows that minimum-energy control can save up to 8% of the energy drawn from the batteries compared with loss-minimization control and up to 6% compared with energy-optimal trapezoidal velocity profile. Because the minimum-energy velocity profile of Eq. (23) resembles a trapezoid for a sufficiently long displacement time, the energy-optimal

trapezoidal velocity profile converges to minimum-energy velocity profile and is a near energy-optimal velocity profile for a longer displacement time. However, it expends more energy when frequent velocity changes are required due to obstacles.

Constraints		Total Energy Drawn from the Batteries E_W (J)		
t_f	x_f	*Minimum-Energy*	*Loss-Minimization*	*TRAPE*
2.0s	1.0m	7.26	7.38 (1.65%)	7.70 (6.06%)
5.0s	3.0m	19.07	20.26 (6.24%)	19.57 (2.62%)
10.0s	5.0m	24.26	26.22 (8.08%)	24.57 (1.27%)
20.0s	10.0m	46.56	49.38 (6.06%)	46.85 (0.62%)
30.0s	15.0m	68.92	71.91 (4.34%)	69.20 (0.41%)

Table 2. Comparison of energy saving for various t_f and x_f

Compared with loss-minimization control, minimum-energy control has a significant energy saving for a displacement time greater than 2s. For a further investigation, we performed a careful analysis of two optimization problems: minimum-energy control and loss-minimization control. Fig. 6 shows the simulations for various time constants τ_v that were performed for t_f = 10.0s and x_f = 5.0m. As the energy-optimal velocity profile depends on $k = \tau_v / t_f$, as shown in Fig. 5, the mechanical time constant affects the velocity profiles of the two optimization problems with different cost functions.

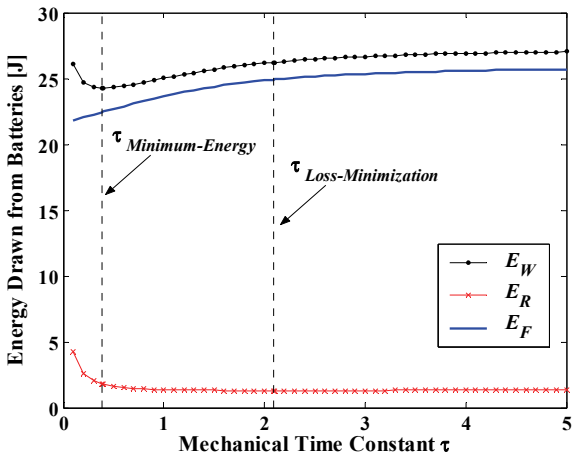

Figure 6. Cost function plot with respect to mechanical time constant τ

Applying the Pontryagin's Maximum Princple to optimize the cost function, the mechanical time constants are $\tau_v = (J_1 + J_2) / \sqrt{F_v (F_v + K_t K_b n^2 / R_a)}$ for minimum-energy control and $\tau_v = (J_1 + J_2) / F_v$ for loss-minimization control. Fig. 6 shows the change of the cost function with respect to various mechanical time constant τ.

From Eq. (2), decreasing the armature current increases the value of the back-emf and the motor speed. Because the mechanical time constant of minimum-energy control less than that of loss-minimization control, the armature current in minimum-energy control quickly

decreases, as shown in Fig. 7(c) during acceleration and deceleration. Hence minimum-energy control can accelerate and decelerate at a higher acceleration rate as shown in Fig. 7(a). Corresponding control inputs are shown in Fig. 7(b) and energy consumptions for each case are shown in Fig. 7(d).

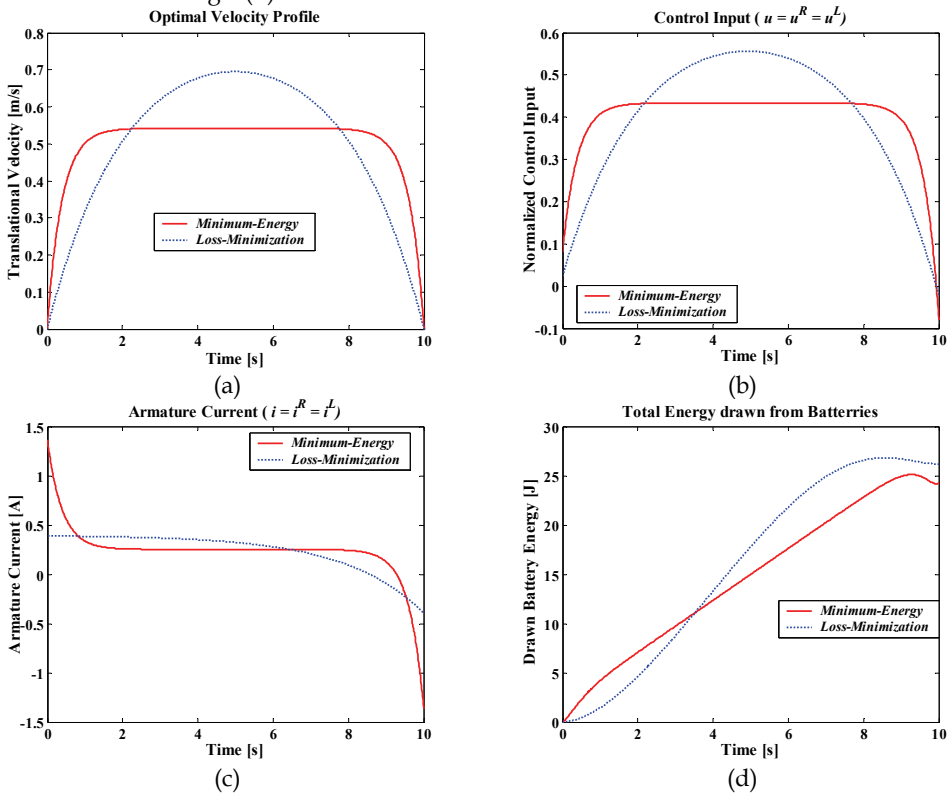

Figure 7. Simulations of minimum-energy control and loss-minimization control for t_f = 10.0s and x_f = 5.0m, (a) Optimal velocity profile, (b) Corresponding control inputs, (c) Armature current change, (d) Comparison of energy consumption

Table 3 shows the ratio of consumed energy for each energy component of Eq. (10) with respect to total energy drawn from the batteries during the entire process for minimum-energy control. Note that the kinetic energy acquired at start up is eventually lost to the whole process when the final velocity is equal to the initial velocity, as shown in Table 3.

t_f	x_f	E_W(%)	E_R (%)	E_F (%)	E_K (%)
2.0s	1.0m	7.26	2.30 (31.68%)	4.96 (68.32%)	0.00 (0.00%)
5.0s	3.0m	19.07	2.35 (12.32%)	16.72 (87.68%)	0.00 (0.00%)
10.0s	5.0m	24.26	1.82 (7.50%)	22.44 (92.50%)	0.00 (0.00%)
20.0s	10.0m	46.56	2.51 (5.39%)	44.05 (94.61%)	0.00 (0.00%)
30.0s	15.0m	68.92	3.26 (4.73%)	65.66 (95.27%)	0.00 (0.00%)

Table 3. Ratio of energy consumption of each energy component for minimum-energy control

Since most of the battery energy is dissipated by the armature resistance for a short displacement time, the minimum-energy control does not have significant energy savings for a short displacement time but shows significant energy savings for a long displacement time, as shown in Table 2.

Fig. 8 shows the power consumption for each energy component of minimum-energy control and loss-minimization control for the constraints given in Fig. 7. It shows that the minimum-energy control requires greater energy consumption than loss-minimization control during accleleration, whereas minimum-energy control consumes less energy after accleration. It means that even though the minimum-energy control requires larger energy consumption than loss-minimization control druing acceleration, it consumes less energy after acceleration. During deceleration a certain amount of energy is *regenerated* and stored in the batteries: 0.94J for minimum-energy control and 0.62J for loss-minimization control.

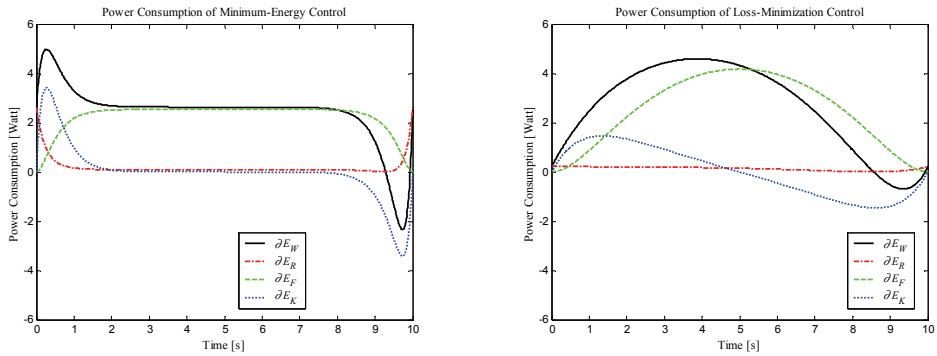

(a) (b)

Figure 8. Comparison of power consumption for each energy component, (a) Minimum-energy control, (b) Loss-minimization control

3.3.2 Experimental Environment Setup

Figure 9. The Pioneer 3-DX robot with a laptop computer

To validate the energy saving of the proposed minimum-energy control, we performed experiments with an actual robot. We use a commercial mobile robot, P3-DX. Fig. 9 is a picture of P3-DX with a laptop computer.
The robot is powered by rechargeable batteries with 12V and has two DC motors with encoders driving two wheels. The maximum translational velocity is approximately 1.2m/s. A Renesas SH2-7144 RISC microcontroller is used to control motors and it communicates with PC client through RS232 serial port. The microcontroller is managed by an Advanced Robot Control and Operations Software (ActiveMedia, 2006).

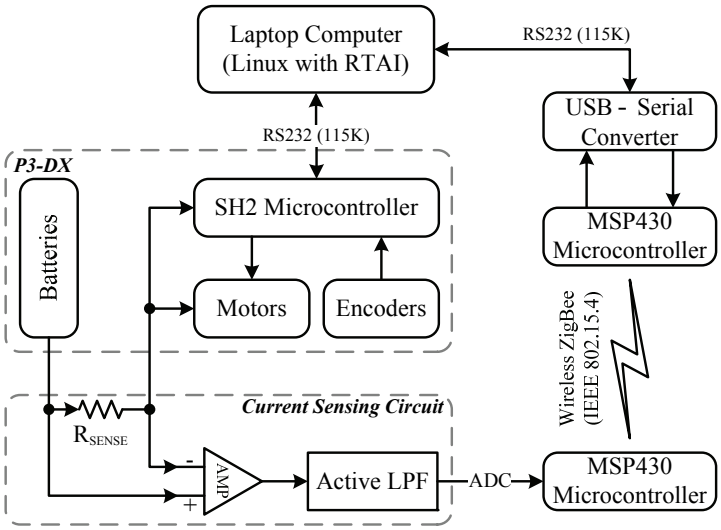

Figure 10. Experimental environment setup

Fig. 10 shows our experimental environment setup. The laptop computer is used to control the robot and to measure the current drawn from the batteries for calculating energy consumption. The robot is controlled by acceleration rate and desired velocity as control commands, and robot's velocity profile is piecewise linear. Since the velocity profiles of minimum-energy and loss-minimization control are nonlinear, we approximated them to piecewise linear velocity profile with 10ms sampling time. The laptop computer is connected to the robot through a serial port with 115Kbps baud rate, and sends a set of acceleration rate and desired velocity of approximated piecewise linear velocity profile to the robot every control period of 10ms, and receives a Standard Information Packet (ActiveMedia, 2006) including velocity and position from the robot every 10ms. Since it is difficult to control every 10ms in Windows or general Linux, we adopted Real-Time Application Interface (RTAI), one of Linux real-time extension, as an operating system of the laptop computer for real-time control (Lineo, 2000).
To measure the drawn energy from the batteries, we sense high side battery current using bi-directional current sensing circuit as shown in Fig. 10. We monitor the current through R_{SENSE} using LT1787 current sense amplifiers with 1.25V reference and filter output of amplifier to obtain average output with unity gain Sallen-Key 2nd order active low pass filter with 1KHz cut-off frequency and unity damping ratio. Then MSP430 microcontroller samples the filtered output with 200Hz sampling rate using 12-bit ADC and transmits

sampled array data to the laptop computer energy 10ms. Since the measured current includes current drawn by microcontroller as well as current drawn by motors, we subtract the measured current when the robot is in initial stop state to obtain the current drawn by motor driving. Fig. 11 shows the bi-directional battery current sensing hardware.

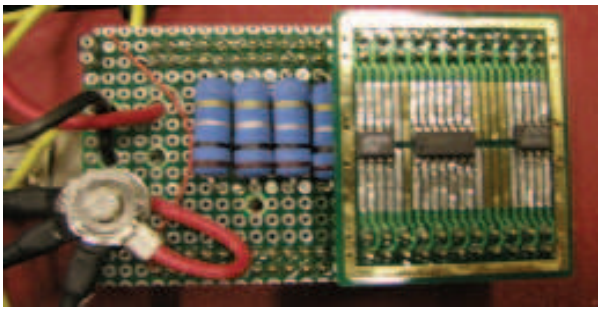

(a)

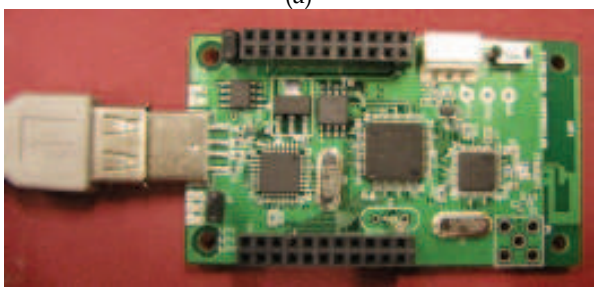

(b)

Figure 11. Battery current sensing hardware, (a) Bi-directional current sensing circuit, (b) MSP430 microcontroller with 12-bit ADC for data acquisition with USB-to-Serial converter

3.3.3 Experiments

We performed experiments for the constraints in Table 2 and compared with loss-minimization control. To calculate energy consumption, we calculated the armature current and the applied voltages of each motor using the ratio of the armature current between two motors since we can only measure the batteries' current of P3-DX. The ratio of the armature currents can be obtained from Eqs. (3) and (5) using measured velocity of WMR as follows.

$$\rho = \frac{i^R}{i^L} = \frac{(J_1 + J_2)\dot{v} + b(J_1 - J_2)\dot{\omega} + F_v(v + b\omega)}{(J_1 + J_2)\dot{v} + b(J_2 - J_1)\dot{\omega} + F_v(v - b\omega)} \tag{24}$$

Since battery current is $i^B = i^R + i^L$, the armature current of two motors are

$$i^R = \frac{\rho}{\rho + 1} i^B, \; i^L = \frac{1}{\rho + 1} i^B \tag{25}$$

and applied voltages of two motors is obtained from Eq. (2). Then we can calculate the drawn energy from the batteries, Eq. (7).

Figs. 12 and 13 show the experimental results that were performed for t_f = 10.0s and x_f = 5.0m compared with simulation results. Actual velocity of the robot follows well desired velocity. Since we ignore the armature inductance of the motor, armature current change and power consumption has slightly different change during accleration and deceleration. However, they show the similar overall response.

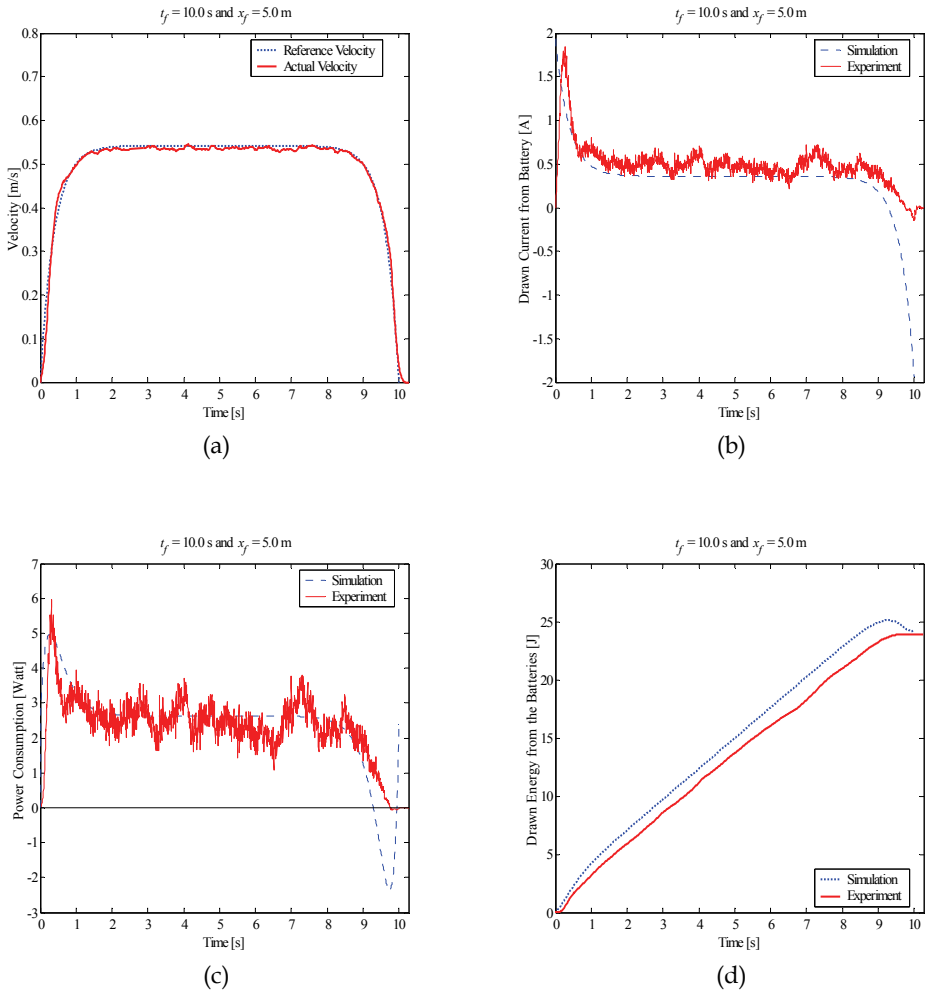

Figure 12. Experimental results of minimum-energy control for t_f = 10.0s and x_f = 5.0m, (a) Velocity profile, (b) Armature current change, (c) Power consumption, (d) Energy consumption

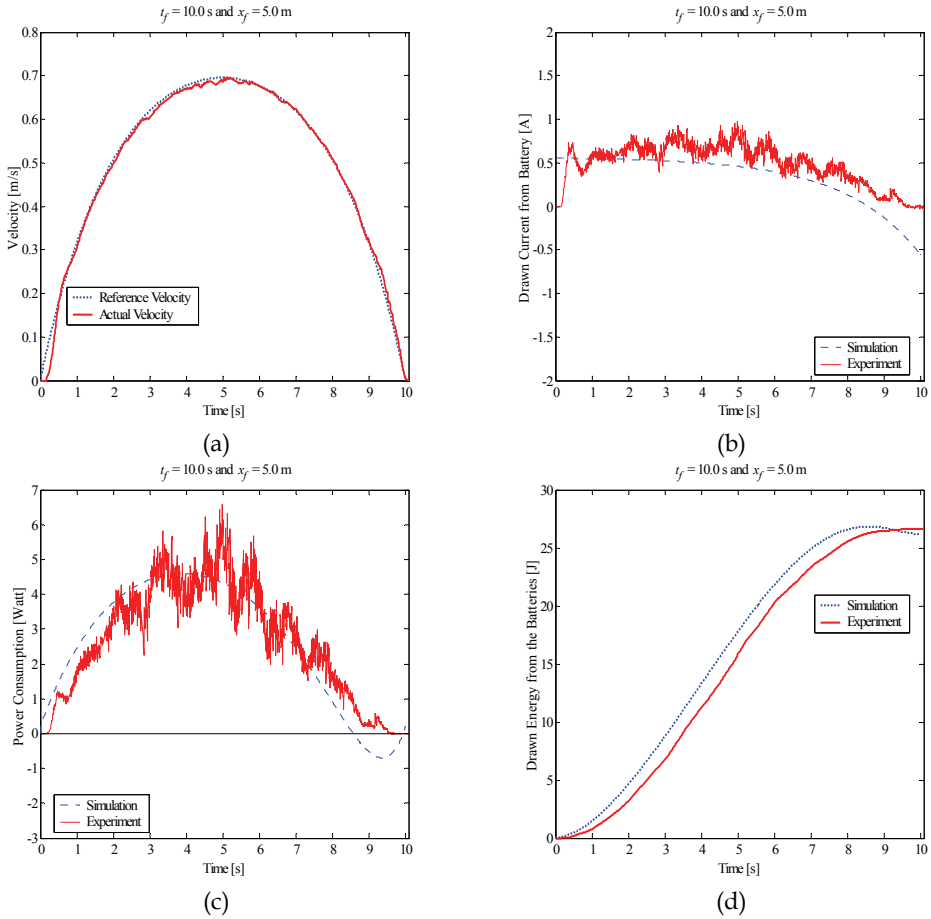

Figure 13. Experimental results of loss-minimization control for t_f = 10.0s and x_f = 5.0m, (a) Velocity profile, (b) Armature current change, (c) Power consumption, (d) Energy consumption

Table 4 shows the experimental results for energy savings for various displacements x_f and displacement time t_f. Values in parenthesis represent percentage difference in the total energy drawn from the batteries with respect to that of minimum-energy control. Experimental results revealed that the minimum-energy control can save up to 11% of the energy drawn from the batteries compared with loss-minimization control.

Since we ignore the inductance of the motors and there can be errors in modelling and measuring the energy drawn from the batteries for experiments is slightly different to that of simulations. However, we can see that the minimum-energy control can save the battery energy compared with loss-minimization control in both experiments and simulations. Table 4 also shows that the percent of energy savings difference between minimum-energy control and loss-minimization control has a similar tendency with that of simulation results in Table 2.

Thank You for previewing this eBook

You can read the full version of this eBook in different formats:

- HTML (Free /Available to everyone)
- PDF / TXT (Available to V.I.P. members. Free Standard members can access up to 5 PDF/TXT eBooks per month each month)
- Epub & Mobipocket (Exclusive to V.I.P. members)

To download this full book, simply select the format you desire below

Free-eBooks.net